New Astronomy 128 (2026) 102622

Contents lists available at ScienceDirect

New Astronomy

journal homepage: www.elsevier.com/locate/newast

# SEVAN network observations of the complex Forbush decrease on 1–2 June 2025

T. Karapetyan *, A. Chilingarian, B. Sargsyan

*Yerevan Physics Institute, Alikhanyan Brothers 2, Yerevan 36, Armenia*

ARTICLE INFO

*Keywords:*
Forbush decrease
SEVAN network
Coronal mass ejections
Cosmic-ray modulation

ABSTRACT

We present observations of a complex two-step Forbush decrease (FD) recorded by the SEVAN particle detector network during the geomagnetic disturbances of 1–2 June 2025. The event was triggered by successive Earth-directed halo coronal mass ejections (CMEs) launched on 30 and 31 May 2025, which likely interacted during propagation and formed a compound interplanetary CME structure. The associated interplanetary shocks arrived, as indicated by sudden storm commencements (SSCs) at 05:22 UTC on 1 June and 10:19 UTC on 2 June, accompanied by strong enhancements of the interplanetary magnetic field and elevated solar wind speeds exceeding 1100 km $s^{-1}$. The SEVAN network recorded a pronounced two-step FD with significant temporal and spatial variations among detectors at Aragats, Lomnický štít, Musala, and Milešovka. Neutron monitors showed smooth global suppression of cosmic rays, while muon channels exhibited additional short-term structures likely associated with transient variations in geomagnetic cutoff rigidity during magnetospheric reconfiguration. Comparison with recent statistical studies of radio-loud CME-driven FDs shows that the June 2025 event exhibits the characteristic signatures of highly geoeffective halo CME disturbances, including rapid propagation, strong magnetic compression, complex FD morphology, and prolonged recovery. These observations demonstrate the SEVAN network's capability to investigate both heliospheric modulation and local magnetospheric effects during major solar disturbances.

## 1. Introduction

Forbush decreases have been extensively investigated as manifestations of cosmic-ray modulation by interplanetary shocks, magnetic clouds, and CME-driven disturbances. Previous studies have shown that both the turbulent sheath region behind interplanetary shocks and the enhanced magnetic fields within interplanetary coronal mass ejections (ICMEs) contribute significantly to the suppression of galactic cosmic rays (Cane, 2000; Belov, 2008). Statistical analyses have further demonstrated strong relationships between FD magnitude and key solar-wind parameters, including CME speed, interplanetary magnetic field strength, and solar-wind velocity, while the observed amplitudes depend on particle rigidity and detector characteristics (Belov, 2008; Richardson and Cane, 2011). These studies established the physical framework within which modern observations of CME-driven Forbush decreases and associated space-weather disturbances are interpreted.

The SEVAN network (Space Environment Viewing and Analysis Network), as part of the United Nations Basic Space Science (UNBSS) activities, was supported by the International Heliophysical Year 2007 (IHY 2007, Thompson et al., 2009) and the UN Office for Outer Space Affairs. Experts from the Cosmic Ray Division (CRD, Chilingarian et al., 2003) at the Yerevan Physics Institute developed a new hybrid particle detector that measures neutral and charged particles. The network's initial rollout included installations in Croatia, Bulgaria, and India (Chilingarian et al., 2009d). Expansion continued in 2023 with the installation of SEVAN detectors in Slovakia, Germany (Hamburg and Berlin), the Czech Republic, and atop Zugspitze, Germany's highest peak (Chilingarian et al., 2024a). Local SEVAN groups foster a research community in solar physics and high-energy atmospheric physics by analyzing neutrons and muons modulated during violent solar events and recording increased fluxes of electrons and gamma rays during thunderstorms and RREA/TGE events. Currently, 10 SEVAN detectors are operational in Armenia and the highest peaks of Eastern Europe and Germany. Since the project's inception in 2007, the SEVAN network has provided valuable data on solar events throughout the highly active 23rd solar activity cycle (Chilingarian et al., 2018). During the relatively weak 24th solar activity cycle, the SEVAN network was extensively utilized for atmospheric physics research, uncovering new sources of

* Corresponding author at: A I Alikhanyan National Science Laboratory, Armenia.
*E-mail address:* ktigran79@gmail.com (T. Karapetyan).

https://doi.org/10.1016/j.newast.2026.102622
Received 20 May 2026; Received in revised form 9 July 2026; Accepted 12 July 2026
Available online 12 July 2026

natural radiation (Chilingarian et al., 2010; 2011; 2024a; Chum et al., 2020) and estimating maximum values of atmospheric electric fields (Chilingarian et al., 2021a; 2021b). The latest discovery was a significant increase in gamma radiation during winter snowstorms (Chilingarian et al., 2025a). The Forbush decreases (FDs, Forbush, 1954) of Solar Cycle 25 observed by the SEVAN network were previously reported by Karapetyan et al. (2024). Recent statistical studies further demonstrated that the strength of FDs depends on the properties of CME-driven interplanetary disturbances. In particular, radio-loud (RL) CMEs associated with type II radio bursts were shown to produce systematically larger FDs than radio-quiet (RQ) CMEs, owing to their higher velocities, wider angular widths, stronger interplanetary magnetic fields, and more intense solar wind disturbances. Bhatt and Chandra (2026) analyzed 195 FD events during Solar Cycle 23 and found that RL CMEs exhibit significantly stronger correlations with IMF Bmax ($r \approx 0.74$), solar wind speed ($r \approx 0.68$), and shorter CME–FD transit times than RQ events, confirming the dominant role of strong CME-driven shocks in producing extreme cosmic-ray depressions. The extreme Forbush decrease observed on 1 June 2025 during Solar Cycle 25 represents an important modern example of such highly geoeffective CME activity. Chilingarian, Karapetyan, and Sargsyan (2025b) reported a pronounced two-step FD structure recorded by SEVAN detectors at Aragats and Lomnický štít, associated with successive halo CMEs, strong interplanetary magnetic field enhancement, and elevated solar wind speed. The event included an SSC at 05:22 UTC on 1 June 2025, IMF enhancement above 24 nT, solar wind speeds exceeding 1100 km $s^{-1}$, and a geomagnetic storm with Dst reaching approximately −122 nT (World Data Center for Geomagnetism, Kyoto et al., 2015; Sugiura, 1964). Independent confirmation of this event was later obtained using the Rozhen mini-neutron monitor and Musala SEVAN detector system. Arsov et al. (2026) demonstrated good agreement between neutron monitor and SEVAN observations of the June 2025 FD and emphasized the role of geomagnetic cutoff rigidity in interpreting detector response during strong interplanetary disturbances. These recent studies provide an opportunity to compare individual extreme events of Solar Cycle 25 with the statistical behavior established for RL CMEs during earlier solar cycles and strengthen the interpretation that strong CME-driven shocks and magnetic disturbances are the primary drivers of large Forbush decreases.

With the maximum of the 25th solar activity cycle reached, SEVAN provides crucial information about the types of solar events and the energy of primary solar protons (Chilingarian et al., 2024c; 2024d). We have already published a brief report comparing magnetospheric and ground-level enhancement events from November 5, 2023, and May 11, 2024 (Chilingarian, 2024). Here, we present SEVAN network observations of a large FD, which occurred on 1–2 June 2025.

## 2. Solar and interplanetary sources

On May 29, 2025, a G3-level geomagnetic storm began, driven by a coronal hole high-speed stream (CH HSS) that rotated into a geoeffective position, sending fast solar wind toward Earth. As the stream progressed, it encountered a co-rotating interaction region (CIR), a compression zone between slow and fast solar wind, leading to an unexpectedly strong geomagnetic disturbance. On May 30, Active Region 4100 produced a significant M3.4-class solar flare at 12:53 UTC, launching a moderately fast halo CME directed toward Earth. This CME was preceded by an earlier CME launched at 06:38 UTC, and the two events likely merged during propagation, forming a compound ICME. The shock from this compound CME system was detected at 05:22 UTC on June 1 by the ACE and DSCOVR spacecraft at the L1 point. Its arrival was marked by a sharp increase in interplanetary magnetic field strength ($B_{total}$) from approximately 7 nT to above 24 nT, along with a surge in solar wind speed from approximately 700 km/s (already elevated due to the CH HSS) to over 1100 km/s. According to USGS, this SSC marked the onset of a severe geomagnetic storm, with Dst plunging to –122 nT by 10:07 UTC. The passage of this interplanetary shock initiated the first phase of the Forbush Decrease (FD), characterized by a sudden drop in cosmic-ray flux with a complex temporal structure. On May 31, the Sun displayed increased activity, with five active regions on its Earth-facing hemisphere. AR4100 alone produced three M-class flares, the most powerful being an M8.2-class flare at 00:05 UTC. This eruption launched a rapid halo CME with an estimated speed of 1900 km/s. The interplanetary shock from this CME reached Earth at 10:19 UTC on June 2, marked by another sharp increase in $B_{total}$ from 6.5 to 24 nT at speeds between 650 and 850 km/s. The arrival of this CME intensified the ongoing geomagnetic storm to G4-level severity. The fast May 31 CME likely overtook the earlier, slower CMEs from May 30, creating a complex interplanetary CME (ICME) structure. This event triggered the second, deeper phase of the Forbush Decrease, aligning with the second minimum in cosmic-ray flux. The combination of multiple CMEs, some of which overtook each other on their way to Earth, resulted in an unusually deep and prolonged FD with a highly structured temporal evolution. The recovery phase lasted nearly a week, and global particle flux measurements showed complex spatial-temporal patterns, indicating large-scale heliospheric structuring and persistent disturbances in the interplanetary magnetic field. To place the June 1–2, 2025 event into a broader heliophysical context, we compare its principal interplanetary and geomagnetic characteristics with the statistical properties of radio-loud (RL) CME-driven Forbush decreases established by Bhatt and Chandra (2026). The comparison demonstrates that the June 2025 event exhibits all major signatures of extreme RL-CME activity: halo and compound CME structure, rapid propagation, strong interplanetary magnetic field enhancement, elevated solar wind speed, short CME–FD delay, and a pronounced two-step FD profile. Although the FD amplitude (~8%) was smaller than the most extreme Solar Cycle 23 events, its interplanetary and geomagnetic parameters fall well within the range of highly geoeffective RL CMEs. Table 1 summarizes this comparison and shows that the June 2025 event represents a modern Solar Cycle 25 counterpart of the strongest RL-CME-driven Forbush decreases identified in previous statistical studies.

Although the June 2025 event exhibited many of the characteristic signatures of highly geoeffective RL CMEs, including halo/compound CME morphology, rapid propagation, elevated solar wind speed, and strong geomagnetic response, its FD amplitude remained smaller than the most extreme Solar Cycle 23 events reported by Bhatt and Chandra (2026). This difference is not unexpected because FD magnitude depends not only on CME geoeffectiveness but also on the strength and spatial extent of the magnetic obstacle responsible for cosmic-ray

**Table 1**
Comparison of the principal characteristics of the June 1–2, 2025, Forbush decrease with the statistical properties of radio-loud CME-driven Forbush decreases during Solar Cycle 23 reported by Bhatt and Chandra (2026). The June 2025 event exhibits the characteristic signatures of extreme RL-CME activity, including halo/compound CMEs, strong IMF enhancement, elevated solar wind speed, rapid onset after SSC, and a complex two-step FD structure.

| Parameter | RL CME statistics (Bhatt and Chandra 2026) | June 1, 2025 FD event |
|---|---|---|
| FD magnitude | up to 28% | ~8%(SEVAN), ~15% (ArNM) |
| CME type | predominantly halo RL CMEs | halo/compound CMEs |
| CME speed | mean ~1300 km/*S, maxima* >2500 km/s | ~1900 km/s second CME |
| IMF Bmax | strong correlation with FD, maxima ~62 nT | ~24 nT |
| Solar wind speed | strong correlation with FD, maxima ~1876 km/s | >1100 km/s |
| CME–FD delay | shorter delays produce larger FDs | rapid onset after SSC |
| FD structure | often complex during strong RL events | clear two-step FD |
| Geomagnetic response | strong interplanetary disturbance | Dst ≈ −122 nT |

modulation. In the June 2025 event, the maximum interplanetary magnetic field reached approximately 24 nT, whereas the largest RL-CME-driven FDs of Solar Cycle 23 were associated with IMF enhancements exceeding 50–60 nT. Likewise, the observed solar wind speed (>1100 km s$^{-1}$), although exceptionally high, remained below the most extreme values reported for RL CMEs (~1800 km s$^{-1}$). Therefore, the event occupied the upper portion of the RL-CME parameter space without reaching the extreme end represented by the largest FD events.

In addition, the observed FD amplitude depends on detector characteristics, geomagnetic cutoff rigidity, and the energy range of the detected particles. Neutron monitors, which respond primarily to lower-rigidity galactic cosmic rays, generally record larger decreases than muon detectors sensitive to higher-energy primaries. This behavior is evident in the present event, where the Aragats neutron monitor recorded a decrease of approximately 15%, whereas the SEVAN upper-scintillator channels showed amplitudes near 8%. Differences among stations may also reflect variations in local geomagnetic cutoff rigidity and asymptotic viewing directions during the disturbed magnetospheric conditions. These observations are consistent with the relationship reported by Bhatt and Chandra (2026), who showed that FD magnitude increases systematically with stronger IMF compression and solar wind disturbances, while detector rigidity and energy response influence the measured amplitude at individual stations.

The comparison further supports the interpretation that the June 2025 event was produced by a strong RL-CME-driven interplanetary disturbance. In both the statistical study of Bhatt and Chandra (2026) and the present event, large FDs are associated with fast halo CMEs, strong IMF enhancement, and elevated solar wind speeds. The June 2025 event also demonstrates the importance of compound CME interactions, in which successive Earth-directed CMEs merge to generate prolonged interplanetary disturbances. This interaction likely contributed to the unusually complex two-step FD structure and week-long recovery phase observed by the SEVAN network.

The geomagnetic response also confirms the event's extreme nature. The Dst depression reaching approximately −122 nT, along with SSC signatures on June 1 and June 2, indicate strong magnetospheric compression and persistent heliospheric turbulence. These conditions efficiently suppress galactic cosmic ray diffusion, producing deep and structured Forbush decreases. Thus, Table 1 not only provides a statistical comparison but also supports the interpretation that the June 2025 event belongs to the class of highly geoeffective RL-CME-driven disturbances discussed in recent Solar Cycle 23 studies.

## 3. SEVAN network response to geomagnetic disturbances

Significant disturbances in the magnetosphere caused large variations in cosmic ray flux, as measured on Earth's surface by neutron monitors and SEVAN detectors. The two-phase Forbush decrease began on June 1 and was extended by successive ICMEs, prolonging the recovery period for a week. Fig. 1 displays the 10-minute averaged count rates from SEVAN detectors with upper 5 cm thick scintillators, located on mountain peaks: Aragats, Armenia (40.25 N, 44.15E, 2000 and 3200 m), Lomnicky Stit, Slovakia (49.2 N, 20.22E, 2634 m), and Musala, Bulgaria (42.1 N, 23.35E, 2930 m). Data from Mileshovka Hill (50.6 N, 13.9E, 837 m) in the Czech Republic is also included. The first FD minimum related to the "cannibal" ICME detected at 05:22 UTC on June 1 shows a minimum of 7.5% consistently at all locations at approximately 15:00 on June 1. The nearly identical amplitudes observed during the first FD minimum are noteworthy because the SEVAN stations operate at different altitudes and geomagnetic cutoff rigidities. Under typical Forbush decrease conditions, stations with lower cutoff rigidities are expected to record larger cosmic-ray depressions. However, during the first phase of the June 2025 event, the modulation appears to have been dominated by the large-scale passage of the compound ICME and its associated shock, producing a relatively uniform suppression of galactic cosmic rays across the rigidity range sampled by the SEVAN network. This result suggests that the first phase of the FD was dominated by large-scale heliospheric modulation, which reduced the differences expected from local rigidity effects. In contrast, the second minimum exhibited clear differences between Aragats and the European stations, indicating the development of spatial anisotropies and increased sensitivity to local cutoff rigidity variations during the more complex stage of the disturbance. This behavior is consistent with a transition from an initially global cosmic-ray depression to a more structured modulation pattern associated with the arrival of the second CME and the evolving compound ICME. The second minimum associated with the M8.2-class flare triggered a rapid halo CME that reached Earth at 10:19 UTC on June 2. The SEVAN network indicates an anisotropy between the European and Aragats detectors. While the Aragats SEVAN shows a shallower minimum, the European SEVAN

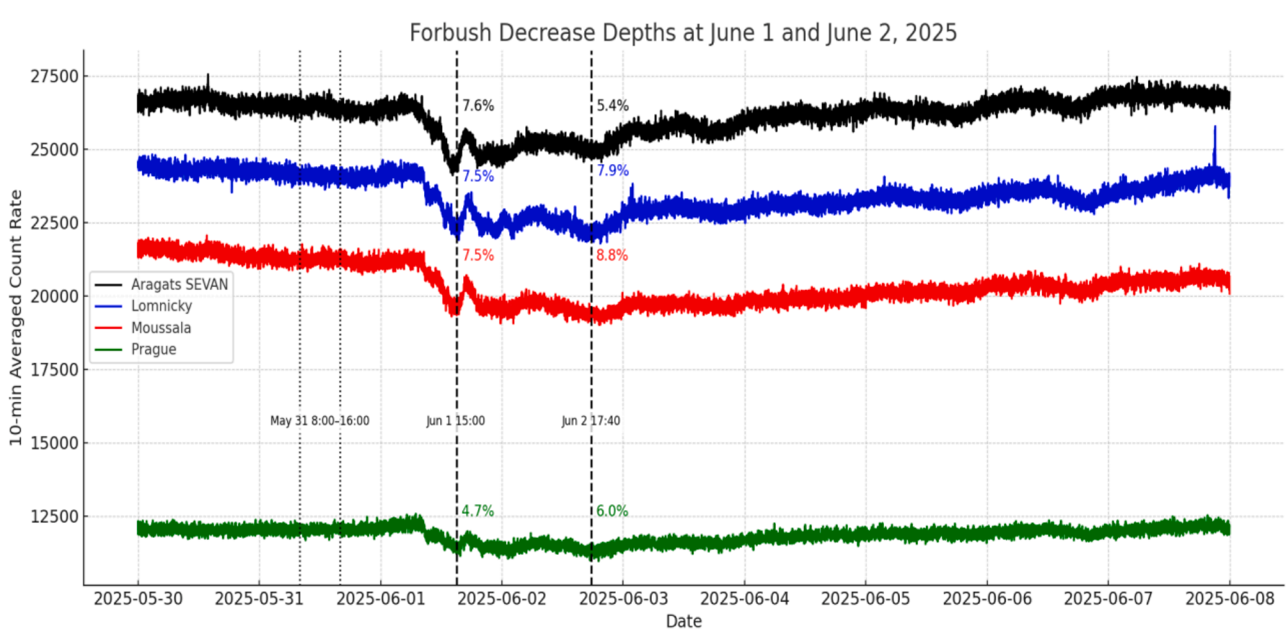


**Fig. 1.** Forbush decrease observed by the upper scintillators SEVAN network. The depletion percentage was calculated relative to the mean values from 8:00 to 16:00 on May 31 (shown by dotted lines). Dashed lines show the deepest depletions of FD.

deepens the particle flux to 7.9% on Lomnicky Stit and 8.8% at Musala at approximately 17:40 on June 2.

Fig. 2 shows the same FD registered by the SEVAN detector, with coincidences selected from samples enriched by neutrons and muons. The Moussala neutrons show the deepest FD at 11%. In contrast, the muon flux (E > 200 MeV) from the Mileshovka SEVAN shows the smallest depletion compared to the mountain SEVANs. All time series from the SEVAN network used in this study were not corrected for atmospheric pressure because pressure measurements were unavailable at all stations during the analyzed period. Nevertheless, the observed Forbush decrease amplitudes (8–15%) substantially exceed the magnitude of typical meteorological variations and exhibit clear temporal correspondence with the arrival times of the interplanetary shocks and geomagnetic disturbances. Therefore, the principal features of the event, including the two-step FD structure and the relative differences among detectors, are interpreted as being primarily of heliospheric and geomagnetic origin.

Neutrons are more sensitive to FD particles. Fig. 3 shows FD measured by Aragats (ArNM) and Nor Amberd (NANM) neutron monitors. Only the Aragats and Lomnicky Stit stations have neutron monitors and SEVAN detectors. The simultaneous detection of solar events by two types of detectors provides a basis for intercalibrating both networks. The ArNM shows a 15% depletion, while the NANM indicates a 2% smaller depletion due to atmospheric cutoff.

Muon detectors with different energy thresholds are very useful for classifying solar events and for assessing the primary solar proton energy during ground-level enhancements (GLEs) and magnetospheric effects (MEs) (Chilingarian et al., 2024b; 2024c). Fig. 4 shows how the STAND3 detector's coincidences (Chilingarian and Hovsepyan, 2023) captured the FD, which separates muons by threshold energy. The STAND3 "1111" coincidence channel, corresponding to muons with energies above 40 MeV according to GEANT4 simulations, exhibits the largest FD amplitude (~12%). This result is somewhat unexpected, as higher-threshold channels are generally expected to show weaker modulation. In general, lower-rigidity primary cosmic rays are expected to be more strongly modulated during FDs. However, the single-layer low-threshold channels contain substantial contributions from electrons and gamma rays, and these soft secondary components are more

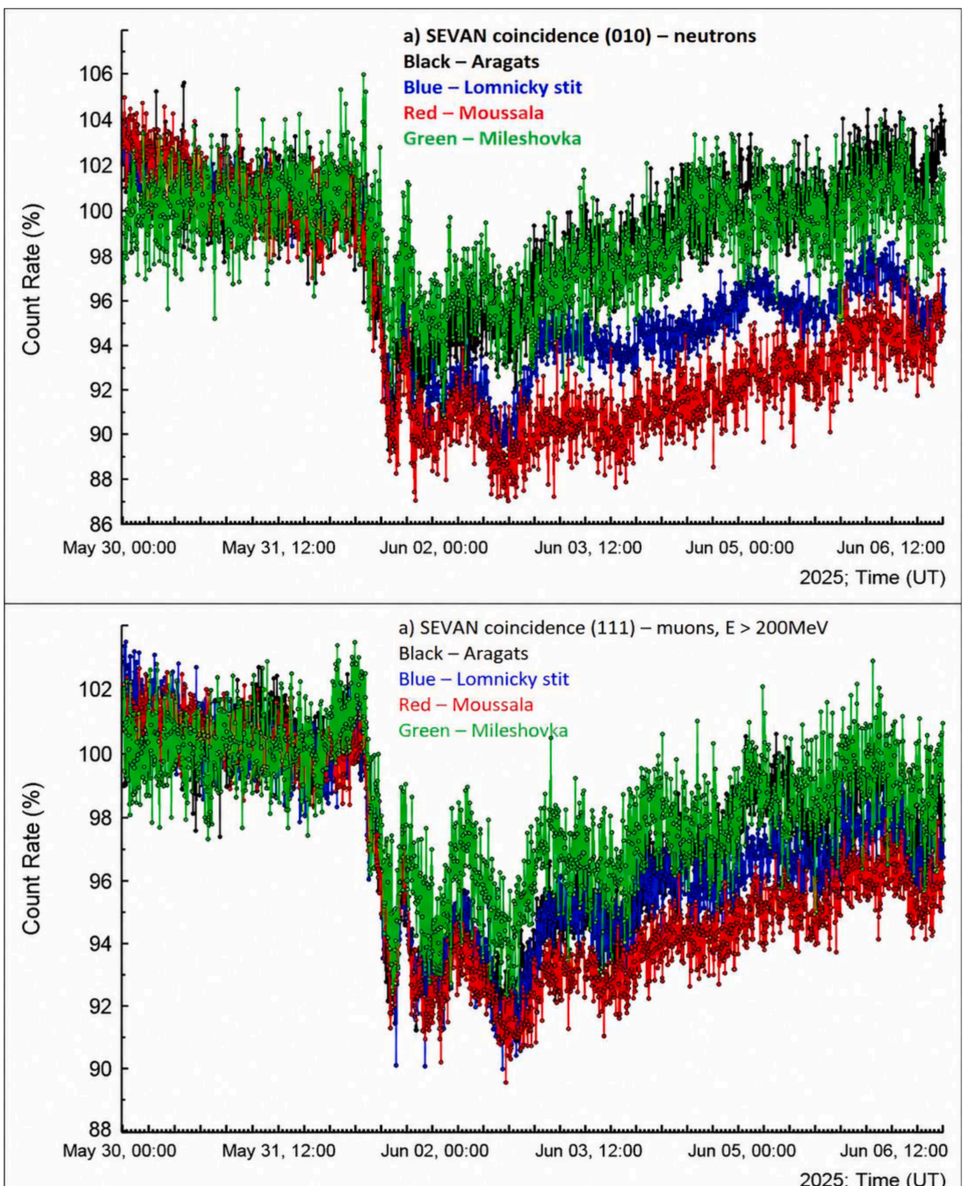


**Fig. 2.** Forbush decrease due to SEVAN coincidences involving selected neutrons and muons. The depletion percentage was calculated relative to the mean values obtained from 8:00 AM to 4:00 PM on May 31.

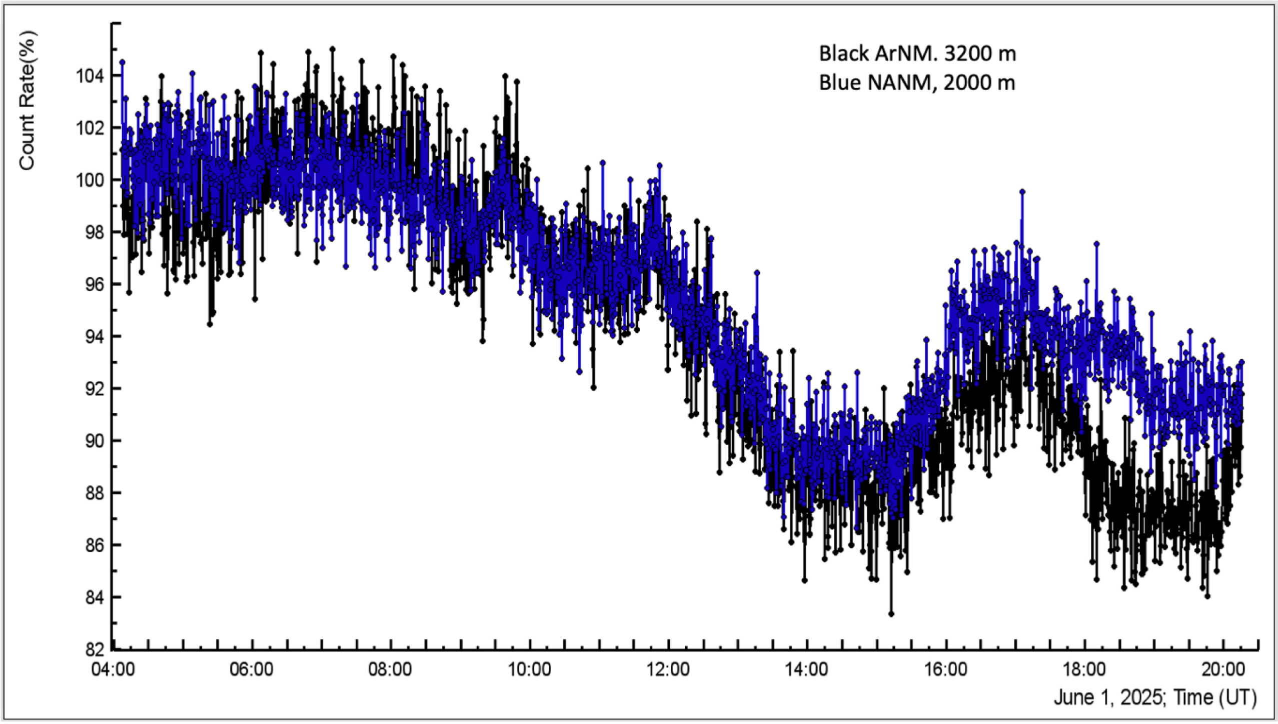


**Fig. 3.** Forbush decrease observed by ArNM (3200 m) and NANM (2000 m).

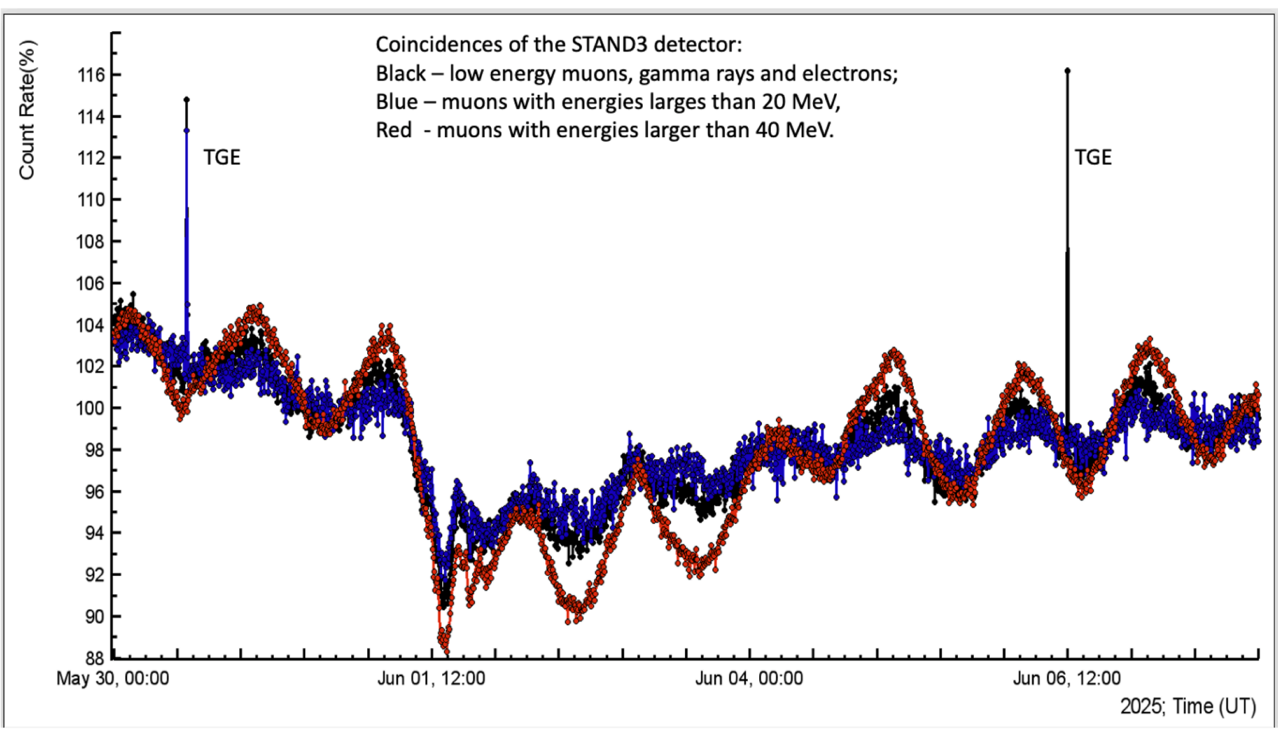


**Fig. 4.** FD registered by the stacked STAND3 detector. The vertical lines indicate TGEs – an impulse enhancement in count rates due to the operation of atmospheric electron accelerators.

strongly affected by local atmospheric and electric-field conditions. This admixture can dilute or distort the FD signature. The '1111' coincidence provides a cleaner muon sample and therefore exhibits a more pronounced FD profile.

In Fig. 4, we also display the thunderstorm ground enhancements (TGEs, Chilingarian et al., 2010, 2011) that occurred during excessive thunderstorms on May 30 and June 6. During thunderstorms, the atmospheric electric field accelerates free electrons. Under specific atmospheric conditions, these electrons form electromagnetic avalanches (cascades of secondary particles initiated by runaway electrons) that reach the surface and are registered as short particle bursts. Detectors with low energy thresholds effectively register such events.

## 4. Discussion and conclusions

The combined neutron and muon observations by the SEVAN network provide complementary insights into the nature of the FD, capturing both global modulation and local dynamic effects. The neutron count rate exhibited a smooth and gradual decrease, characteristic of global cosmic ray suppression by interplanetary magnetic structures. Neutrons are produced by spallation reactions when primary cosmic rays interact with atmospheric nuclei. Neutrons are extremely sensitive to Forbush Decreases because they originate from primary cosmic rays with energies around 1–20 GeV, where the modulation is strongest. Unlike charged particles, neutrons are not affected by magnetic fields once produced, making them an excellent probe of the primary cosmic ray flux variations. Neutron monitors have historically been the primary instruments for detecting Forbush Decreases because they exhibit large-amplitude reductions (10–20% for strong events). In contrast, muon detectors, sensitive to higher-energy primaries (10–1000 GeV), reveal complementary information about both global and local geomagnetic modulation. Meanwhile, detectors sensitive to low-energy electrons and gamma rays exhibit weak or unclear FD signals due to strong atmospheric and environmental background contamination. The muon count rate showed a similar overall FD amplitude, with additional short-term spikes superimposed on the general trend. These muon spikes are interpreted as signatures of magnetospheric effects, likely due to transient variations in the geomagnetic cutoff rigidity during the ongoing geomagnetic field reconfiguration. The larger FD amplitude observed in the neutron-enriched '010′ coincidence, compared with the upper scintillator, can be explained by differences in particle composition and detector response. The upper scintillator records a mixture of muons, electrons, and gamma rays, including numerous soft secondary particles that are weakly affected by heliospheric modulation. In contrast, the '010' coincidence preferentially selects neutral particles because the upper scintillator acts as a veto for charged particles, while the lead absorber suppresses low-energy secondaries. As a result, the neutron-enriched channel provides a cleaner measurement of the modulated cosmic-ray component and exhibits a stronger relative FD amplitude.

## Author statement

All authors have contributed significantly to this work and have approved the final version of the manuscript. The manuscript is original, has not been published previously, and is not under consideration for publication elsewhere. All authors have reviewed and approved the revised manuscript and the responses to the reviewers' comments. The authors declare that there are no conflicts of interest regarding the publication of this paper.

## CRediT authorship contribution statement

**T. Karapetyan:** Writing – original draft, Resources, Investigation, Formal analysis, Data curation. **A. Chilingarian:** Project administration, Methodology, Investigation, Funding acquisition, Conceptualization. **B. Sargsyan:** Visualization, Software, Formal analysis.

## Declaration of competing interest

The authors declare that they have no known competing financial interests or personal relationships that could have appeared to influence the work reported in this paper.

## Acknowledgment

We thank the staff of the Aragats Space Environmental Center for the uninterrupted operation of all experimental facilities on Mount Aragats. The work was supported by the Science Committee of RA within the framework of the research project № 21AG-1C012.

## Data availability

Data will be made available on request.

## References

Arsov, T., Tyutyundzhiev, N., Angelov, Ch, Serafimov, N., Georgiev, G., Petrov, M., 2026. Secondary neutron monitoring at Rozhen observatory - first year report. J. Phys. 3194, 012026. https://doi.org/10.1088/1742-6596/3194/1/012026.

Belov, A., 2008. Forbush effects and their connection with solar, interplanetary and geomagnetic phenomena. Proc. Int. Astron. Union 4 (S257), 439–450.

Bhatt, B., Chandra, H., 2026. Forbush decreases associated with radio-loud and radio-quiet coronal mass ejections in relation to interplanetary parameters during solar cycle 23′. Adv. Space Res 77, 12792–12809. https://doi.org/10.1016/j.asr.2026.04.046.

Cane, H.V., 2000. Coronal mass ejections and forbush decreases. Space Sci. Rev. 93, 55–77.

Chilingarian, A., Hovsepyan, G., 2023. Proving "new physics'' by measuring cosmic ray fluxes. Astron. Comput. 44, 100714. https://doi.org/10.1016/j.ascom.2023.100714.

Chilingarian, A., Avagyan, K., Babayan, V., et al., 2003. Aragats Space- Environmental Center: status and SEP forecasting possibilities. J. Phys, G Nucl., Part Phys. 29, 939–951. https://doi.org/10.1088/0954-3899/29/5/314.

Chilingarian, A., Avakyan, K., Arakelyan, K., et al., 2009d. Space environmental viewing and analysis network (SEVAN). Earth Moon Planets. 104, 195–210. https://doi.org/10.1007/s11038-008-9288-1.

Chilingarian, A., Daryan, A., Arakelyan, K., Hovhannisyan, A., Mailyan, B., Melkumyan, L., Hovsepyan, G., Vanyan, L., 2010. Ground-based observations of thunderstorm-correlated fluxes of high-energy electrons, gamma rays, and neutrons. Phys. Rev. D 82, 043009. https://doi.org/10.1103/PhysRevD.82.043009.

Chilingarian, A., Hovsepyan, G., Hovhannisyan, A., 2011. Particle bursts from thunderclouds: natural particle accelerators above our heads. Phys. Rev. D 83, 062001. https://doi.org/10.1103/PhysRevD.83.062001.

Chilingarian, A., Babayan, V., Karapetyan, T., et al., 2018. The SEVAN Worldwide network of particle detectors: 10 years of operation. Adv. Space Res. 61, 2680–2696.

Chilingarian, A., Nikolova, N., Chum, J., Langer, R., 2021a. Maximum strength of the atmospheric electric field in thunderclouds. Phys. Rev. D 103, 043021. https://doi.org/10.1103/PhysRevD.103.043021.

Chilingarian, A., Hovsepyan, G., Karapetyan, G., Zazyan, M., 2021b. Stopping muon effect and estimation of intracloud electric field. Astropart. Phys. 124, 102505. https://doi.org/10.1016/j.astropartphys.2020.102505.

Chilingarian, A., Karapetyan, T., Sargsyan, B., Knapp, J., Walter, M., Rehm, T., 2024a. Energy spectra of the first TGE observed on Zugspitze by the SEVAN light detector compared with the energetic TGE observed on Aragats. Astropart. Phys. 156, 102924. https://doi.org/10.1016/j.astropartphys.2024.102924.

Chilingarian, A., Karapetyan, T., Sargsyan, B., Zazyan, M., Knapp, J., Walter, M., Rehm, T., 2024b. Increase in the count rates of ground-based cosmic-ray detectors caused by the heliomagnetic disturbance on 5 November 2023. EPL 146, 24001. https://doi.org/10.1209/0295-5075/ad329c.

Chilingarian, A., Karapetyan, T., Sargsyan, B., Asatryan, K., Gabaryan, G., 2024c. Influence of interplanetary coronal mass ejections on terrestrial particle fluxes through magnetosphere disturbances. EPL 148, 19001. https://doi.org/10.1209/0295 5075/ad7e4c.

Chilingarian, A., Aslanyan, D., Sargsyan, B., Kozliner, L., 2025a. Wind-induced natural gamma radiation. EPL 151 (1), 14001. https://doi.org/10.1209/0295-5075/ade562.

Chilingarian, A., Karapetyan, G., Sargsyan, B., 2025b. The largest Forbush decrease of solar cycle 25 observed by the SEVAN network. arXiv: 2506.17917. https://arxiv.org/abs/2506.17917#:~:text=https%3A//doi.org/10.48550/arXiv.2506.17917.

Chilingarian, A., 2024. The solar modulation events of the 25th solar activity cycle as seen by particle detectors' Networks, letters of solar influences on the magnetosphere. Ionos. Atmos 1, 1–13. https://doi.org/10.31401/WSL2024.1.

Chum, R.Langer, Baše, J., Kollárik, M., Strhárský, I., Diendorfer, G., Rusz, J., 2020. Significant enhancements of secondary cosmic rays and electric field at high mountain peak during thunderstorms. Earth Planets Space. 72, 28. https://doi.org/10.1186/s40623-020-01155-9.

Forbush, S., 1954. World-wide cosmic-ray variations in 1937-1952. J. Geophys., Res. 59 (4), 525–542.

Karapetyan, T., Chilingarian, A., Hovsepyan, G., et al., 2024. The Forbush decrease observed by the SEVAN particle detector network in the 25th solar activity cycle. J. Atmos. Sol.-Terr. Phys. 262, 106305.

Kyoto, Nose M., Iyemori T., Sugiura M. and Kamei T., World data center for geomagnetism, (2015) Geomagnetic Dst index, doi:10.17593/14515-74000.

Richardson, I.G., Cane, H.V., 2011. Galactic cosmic ray intensity response to interplanetary coronal mass ejections/magnetic clouds in 1995–2009. Sol Phys. 270, 609–627.

Sugiura, M., 1964. Hourly values of equatorial dst for the IGY. Ann. Int. Geophys. Year 35, 9. Pergamon Press, Oxford.

Thompson, B.J., Gopalswamy, N., Davila, J.M., Haubold, H.J. (Eds.), 2009. Putting the "I" in IHY: The United Nations Report For the International Heliophysical Year 2007. Springer, Vienna, Austria.